Aerospace Science and Technology 68 (2017) 391–402

Contents lists available at ScienceDirect

Aerospace Science and Technology

www.elsevier.com/locate/aescte

Static response and free vibration of functionally graded carbon nanotube-reinforced composite rectangular plates resting on Winkler–Pasternak elastic foundations

Nguyen Dinh Duc [a,b], Jaehong Lee [c], T. Nguyen-Thoi [d,e], Pham Toan Thang [d,e,*]

[a] Advanced Materials and Structures Laboratory, VNU-Hanoi, University of Engineering and Technology, 144 Xuan Thuy, Cau Giay, Hanoi, Viet Nam
[b] Infrastructure Engineering Program, VNU-Hanoi, Vietnam–Japan University (VJU), My Dinh 1, Tu Liem, Hanoi, Viet Nam
[c] Department of Architectural Engineering, Sejong University, 209 Neungdong-ro, Gwangjin-gu, Seoul 143-747, Republic of Korea
[d] Division of Computational Mathematics and Engineering, Institute for Computational Science, Ton Duc Thang University, Ho Chi Minh City, Viet Nam
[e] Faculty of Civil Engineering, Ton Duc Thang University, Ho Chi Minh City, Viet Nam

ARTICLE INFO

Article history:
Received 23 February 2017
Received in revised form 15 May 2017
Accepted 23 May 2017
Available online 29 May 2017

Keywords:
Carbon nanotube
Functionally graded materials
Static response
Free vibration
Analytical solution
First-order shear deformation theory

ABSTRACT

In the present article, static response and free vibration of functionally graded carbon nanotube reinforced composite (FG-CNTRC) rectangular plate resting on Winkler–Pasternak elastic foundations using an analytical approach are studied. The rectangular plates are reinforced by single-walled carbon nanotubes (SWCNTs) which are assumed to be graded through the thickness direction with four types of distributions. The mathematical model of the FG-CNTRC plate is developed based on the first-order shear deformation plate theory (FSDT) and Hamilton principle. By using Navier solution, the governing equations are solved to obtain the central deflection and the natural frequency parameters. Several examples are verified to have higher accuracy than those from the previous method in the literature. Also, the effects of different parameters on static response and natural frequency of FG-CNTRC plate are highlighted by solving numerous examples. Finally, these new results may serve as benchmarks for future investigations.

1. Introduction

Since the discovery of carbon nanotubes (CNTs) in 1991 [1], they have attracted the remarkable attention of researchers and stimulated their imagination in many industries. The theoretical modeling [2–8] and experimental measurements [9–12] have been showed that CNTs possess high tensile modulus and strength and can sustain large elastic strain. Most studies on carbon nanotube-reinforced composites (CNTRCs) have focused on their material properties [13–21].

The concept of functionally graded materials (FGMs) was proposed in 1984 by materials scientists in the Sendai Institute area as a means of preparing thermal barrier materials [22,23]. These materials have received great attention as structural constituents exposed to intense temperature conditions such as aerospace, nuclear plants, and other engineering applications.

Exceptional characteristics of FGMs and CNTs may be obtained together through functionally graded distribution of CNTs. Shen [24] investigated nonlinear bending of functionally graded carbon nanotube-reinforced composite (FG-CNTRC) plates. After the interesting results of this work, various studies are done to investigate the bending, buckling and vibration responses of the FG-CNTRC. Liew et al. have published a series of papers regarding static buckling and post-buckling response [25–27], vibration [28–32] of FG-CNTRC plate based on the finite element method. Based on the isogeometric analysis, Phung-Van et al. [33] studied the static and dynamic behavior of FG-CNTRC plates. Thang et al. [34] presented an analytical solution for nonlinear buckling of imperfect FG-CNTRC plates. Thermal and mechanical stability of FG-CNTRC truncated conical shells were studied by Duc et al. [35]. The postbuckling of FG-CNTRC cylindrical shells in thermal environments was also presented by Shen et al. [36–39]. Ke et al. [40] examined the nonlinear free vibration of FG nanocomposite beams reinforced by single-walled carbon nanotubes (SWCNTs) based on Timoshenko beam theory. Based on theory of elasticity, the static behavior of the FG-CNTRC rectangular host plate attached to thin piezoelectric layers was studied by Alibeigloo [41,42]. Wu and Chan [43] developed a unified formulation of finite layer methods for the

* Corresponding author at: Division of Computational Mathematics and Engineering, Institute for Computational Science, Ton Duc Thang University, Ho Chi Minh City, Viet Nam.
E-mail address: phamtoanthang@tdt.edu.vn (P.T. Thang).

http://dx.doi.org/10.1016/j.ast.2017.05.032
1270-9638/

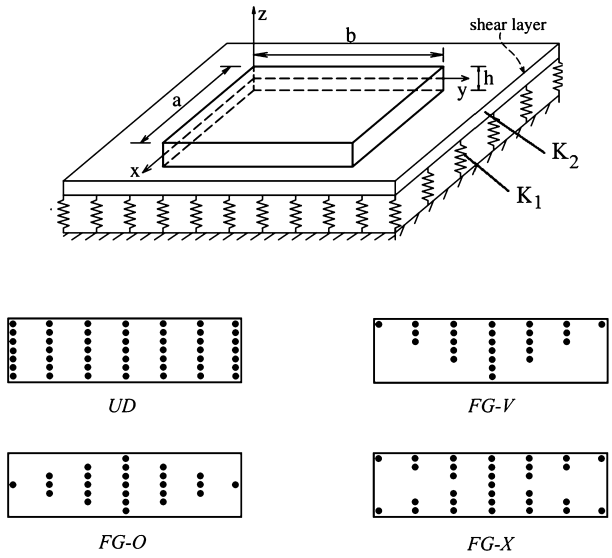

Fig. 1. Geometry and configurations of CNTRC plates resting on Winkler–Pasternak elastic foundations.

three-dimensional buckling behavior of the FG-CNTRC plates with surface-bonded piezoelectric actuator. The forced vibration analysis of FG-CNTRC plates has been in [44], based a numerical strategy. Jalali and Heshmati [45] presented the buckling of circular sandwich plates with tapered cores and FG-CNT face sheets under uniform radial compression. Based the Ritz method, Kiani [46, 47] investigated buckling and free vibration analysis of skew plates made from FG-CNTRC. Recently, Ansari et al. [48] analyzed vibration response of FG-CNTRC elliptical plates based on a numerical strategy.

As seen from the above literature survey and to the best of author's knowledge, there is no work available on the static response and free vibration of FG-CNTRC rectangular plates resting on Winkler–Pasternak elastic foundations based on an analytical solution. Present work aims to fill this gap in the open literature. In this present study, the rectangular plates are reinforced by single-walled carbon nanotubes (SWCNTs) which are assumed to be graded through the thickness direction with four types of distributions. The mathematical model of the FG-CNTRC plate is developed based on the first-order shear deformation plate theory (FSDT) and the Hamilton principle. By applying Navier solution, the governing equation can be solved to obtain the static and vibration responses of simply supported FG-CNTRC plate. Several examples are verified to have higher accuracy than those from the previous method in the literature. Moreover, the effects of CNT volume fraction, plate length-to-thickness ratio, plate length-to-width ratio, and the elastic foundation on static response and natural frequency of CNTRC plate are examined in details. Finally, the results of this study may be useful for other investigations of FG-CNTRC plates.

2. Basic formulation

2.1. Functionally graded carbon nanotubes reinforced composite plates

Consider an FG-CNTRC plate with length a, width b and thickness h as shown in Fig. 1. Polymeric matrix of the composite plate is reinforced with the SWCNTs. Distribution of CNTs in a matrix may be FG or uniform. In this study, three types of FG along with the uniformly distributed case are considered. FG-O, FG-V and FG-X represent the FG distributions of CNTs in the polymeric matrix. The uniform distribution is shown by UD.

In this research, the modified rule of mixtures approach which contains the efficiency parameters is used extensively to extract the elastic properties of FG-CNTRC plate as [24]

$$\begin{aligned} E_{11} &= \eta_1 V_{CNT} E_{11}^{CNT} + V_m E_m \\ \frac{\eta_2}{E_{22}} &= \frac{V_{CNT}}{E_{22}^{CNT}} + \frac{V_m}{E_m} \\ \frac{\eta_2}{G_{12}} &= \frac{V_{CNT}}{G_{12}^{CNT}} + \frac{V_m}{G_m} \end{aligned} \tag{1}$$

where $(E_{11}^{CNT}, E_{22}^{CNT}, G_{12}^{CNT})$ are the Young's and shear modulus of CNT, respectively; (E_m, G_m) are the Young's modulus and shear modulus of the polymeric matrix; (η_1, η_2, η_3) are the CNT efficiency parameters. The volume fraction of CNTs and matrix are denoted by V_{CNT} and V_m, respectively, which can be given by [24]

$$V_{CNT} + V_m = 1 \tag{2}$$

The effective Poisson ratio and mass density depend weakly on position and are expressed as [24]

$$\begin{aligned} \nu_{12} &= V_{CNT}^{*} \nu_{12}^{CNT} + V_m \nu_m \\ \rho &= V_{CNT} \rho_{CNT} + V_m \rho_m \end{aligned} \tag{3}$$

where $(\nu_{12}^{CNT}, \rho^{CNT})$ and (ν_m, ρ_m) are the Poisson's ratio and mass density of CNT and matrix, respectively.

The volume fraction of CNTs as a function of thickness coordinate can be expressed as follows [24]

$$V_{CNT} = \begin{cases} V_{CNT}^{*} & (UD) \\ 2V_{CNT}^{*}(1 - 2\frac{|z|}{h}) & (FG-O) \\ V_{CNT}^{*}(1 + 2\frac{z}{h}) & (FG-V) \\ 4V_{CNT}^{*}\frac{|z|}{h} & (FG-X) \end{cases} \tag{4}$$

where

$$V_{CNT}^{*} = \frac{w_{CNT}}{w_{CNT} + (\rho_{CNT} - \rho_m) - (\rho_{CNT} - \rho_m) w_{CNT}} \tag{5}$$

in which w_{CNT} represents the mass fraction of the CNTs.

2.2. Governing equations

According to the first order shear deformation plate theory, displacement components of the plate may be written in terms of the characteristics of the mid-surface of the plate and cross section rotations as [49]

$$\begin{aligned} u(x, y, z, t) &= u_0(x, y, t) + z\phi_x(x, y, t) \\ v(x, y, z, t) &= v_0(x, y, t) + z\phi_y(x, y, t) \\ w(x, y, z, t) &= w_0(x, y, t) \end{aligned} \tag{6}$$

where (u, v, w) are the displacement components along (x, y, z) coordinates; (u_0, v_0, w_0) are the displacements along the coordinate lines of a material point in the xy-plane; (ϕ_x, ϕ_y) denote the rotations of the transverse normal about the y- and x-axes, respectively.

The strain-displacement relations based the FSDT can be expressed as follows [49]

$$\begin{Bmatrix} \varepsilon_x \\ \varepsilon_y \\ \gamma_{yz} \\ \gamma_{xz} \\ \gamma_{xy} \end{Bmatrix} = \begin{Bmatrix} \varepsilon_x^{(0)} \\ \varepsilon_y^{(0)} \\ \gamma_{yz}^{(0)} \\ \gamma_{xz}^{(0)} \\ \gamma_{xy}^{(0)} \end{Bmatrix} + z \begin{Bmatrix} \kappa_x \\ \kappa_y \\ \kappa_{yz} \\ \kappa_{xz} \\ \kappa_{xy} \end{Bmatrix} \tag{7}$$

where

$$\begin{Bmatrix} \varepsilon_x^{(0)} \\ \varepsilon_y^{(0)} \\ \gamma_{yz}^{(0)} \\ \gamma_{xz}^{(0)} \\ \gamma_{xy}^{(0)} \end{Bmatrix} = \begin{Bmatrix} \frac{\partial u_0}{\partial x} + \frac{1}{2}(\frac{\partial w_0}{\partial x})^2 \\ \frac{\partial v_0}{\partial y} + \frac{1}{2}(\frac{\partial w_0}{\partial y})^2 \\ \frac{\partial w_0}{\partial y} + \phi_y \\ \frac{\partial w_0}{\partial x} + \phi_x \\ \frac{\partial u_0}{\partial y} + \frac{\partial v_0}{\partial x} + \frac{\partial w_0}{\partial x}\frac{\partial w_0}{\partial y} \end{Bmatrix},$$

$$\begin{Bmatrix} \kappa_x \\ \kappa_y \\ \kappa_{yz} \\ \kappa_{xz} \\ \kappa_{xy} \end{Bmatrix} = \begin{Bmatrix} \frac{\partial \phi_x}{\partial x} \\ \frac{\partial \phi_y}{\partial y} \\ 0 \\ 0 \\ \frac{\partial \phi_x}{\partial y} + \frac{\partial \phi_y}{\partial x} \end{Bmatrix} \tag{8}$$

The stress–strain relations may be written as a linear function by the following equation [49]

$$\begin{Bmatrix} \sigma_{xx} \\ \sigma_{yy} \\ \tau_{yz} \\ \tau_{xz} \\ \tau_{xy} \end{Bmatrix} = \begin{bmatrix} Q_{11} & Q_{12} & 0 & 0 & 0 \\ Q_{12} & Q_{22} & 0 & 0 & 0 \\ 0 & 0 & Q_{44} & 0 & 0 \\ 0 & 0 & 0 & Q_{55} & 0 \\ 0 & 0 & 0 & 0 & Q_{66} \end{bmatrix} \begin{Bmatrix} \varepsilon_{xx} \\ \varepsilon_{yy} \\ \gamma_{yz} \\ \gamma_{xz} \\ \gamma_{xy} \end{Bmatrix} \tag{9}$$

where

$$\begin{aligned} Q_{11} &= \frac{E_{11}}{1-\nu_{12}\nu_{21}}, \qquad Q_{22} = \frac{E_{22}}{1-\nu_{12}\nu_{21}}, \\ Q_{12} &= \frac{\nu_{21}E_{11}}{1-\nu_{12}\nu_{21}} \\ Q_{44} &= G_{23}, \qquad Q_{55} = G_{13}, \qquad Q_{66} = G_{12}. \end{aligned} \tag{10}$$

Here (N_x, N_y, N_{xy}) denote the total in-plane force resultants and (M_x, M_y, M_{xy}) the total moment results defined by

$$\begin{Bmatrix} N_x \\ N_y \\ N_{xy} \end{Bmatrix} = \int_{-h/2}^{h/2} \begin{Bmatrix} \sigma_x \\ \sigma_y \\ \sigma_{xy} \end{Bmatrix} dz, \qquad \begin{Bmatrix} M_x \\ M_y \\ M_{xy} \end{Bmatrix} = \int_{-h/2}^{h/2} \begin{Bmatrix} \sigma_x \\ \sigma_y \\ \sigma_{xy} \end{Bmatrix} z dz,$$

$$\begin{Bmatrix} I_0 \\ I_1 \\ I_2 \end{Bmatrix} = \int_{-h/2}^{h/2} \rho \begin{Bmatrix} 1 \\ z \\ z^2 \end{Bmatrix} dz \tag{11}$$

The following motion equations can be obtained as [49]

$$\frac{\partial N_x}{\partial x} + \frac{\partial N_{xy}}{\partial y} = I_0\frac{\partial^2 u_0}{\partial t^2} + I_1\frac{\partial^2 \phi_x}{\partial t^2} \tag{12a}$$

$$\frac{\partial N_{xy}}{\partial x} + \frac{\partial N_y}{\partial y} = I_0\frac{\partial^2 v_0}{\partial t^2} + I_1\frac{\partial^2 \phi_y}{\partial t^2} \tag{12b}$$

$$\begin{aligned} &\frac{\partial Q_x}{\partial x} + \frac{\partial Q_y}{\partial y} + \frac{\partial}{\partial x}\left(\hat{N}_x\frac{\partial w_0}{\partial x} + \hat{N}_{xy}\frac{\partial w_0}{\partial y}\right) \\ &\quad + \frac{\partial}{\partial y}\left(\hat{N}_{xy}\frac{\partial w_0}{\partial x} + \hat{N}_y\frac{\partial w_0}{\partial y}\right) - K_1 w_0 \\ &\quad + K_2\left(\frac{\partial^2 w_0}{\partial x^2} + \frac{\partial^2 w_0}{\partial y^2}\right) + q = I_0\frac{\partial^2 w_0}{\partial t^2} \end{aligned} \tag{12c}$$

$$\frac{\partial M_x}{\partial x} + \frac{\partial M_{xy}}{\partial y} - Q_x = I_1\frac{\partial^2 u_0}{\partial t^2} + I_2\frac{\partial^2 \phi_x}{\partial t^2} \tag{12d}$$

$$\frac{\partial M_{xy}}{\partial x} + \frac{\partial M_y}{\partial y} - Q_y = I_1\frac{\partial^2 v_0}{\partial t^2} + I_2\frac{\partial^2 \phi_y}{\partial t^2} \tag{12e}$$

where the quantities (Q_x, Q_y) are called the transverse force resultants as

$$\begin{Bmatrix} Q_x \\ Q_y \end{Bmatrix} = K\int_{-h/2}^{h/2} \begin{Bmatrix} \sigma_{xz} \\ \sigma_{yz} \end{Bmatrix} dz \tag{13}$$

in which K is called the shear correction coefficient.

The force and moment resultants are related to the generalized displacement $(u_0, v_0, w_0, \phi_x, \phi_y)$ by substituting Eqs. (7), (8) into Eq. (9) and then into Eq. (11), we have

$$\begin{aligned} \begin{Bmatrix} N_x \\ N_y \\ N_{xy} \end{Bmatrix} &= \begin{bmatrix} A_{11} & A_{12} & 0 \\ A_{12} & A_{22} & 0 \\ 0 & 0 & A_{66} \end{bmatrix} \begin{Bmatrix} \frac{\partial u_0}{\partial x} + \frac{1}{2}(\frac{\partial w_0}{\partial x})^2 \\ \frac{\partial v_0}{\partial y} + \frac{1}{2}(\frac{\partial w_0}{\partial y})^2 \\ \frac{\partial u_0}{\partial y} + \frac{\partial v_0}{\partial x} + \frac{\partial w_0}{\partial x}\frac{\partial w_0}{\partial y} \end{Bmatrix} \\ &\quad + \begin{bmatrix} B_{11} & B_{12} & 0 \\ B_{12} & B_{22} & 0 \\ 0 & 0 & B_{66} \end{bmatrix} \begin{Bmatrix} \frac{\partial \phi_x}{\partial x} \\ \frac{\partial \phi_y}{\partial y} \\ \frac{\partial \phi_x}{\partial y} + \frac{\partial \phi_y}{\partial x} \end{Bmatrix} \end{aligned} \tag{14}$$

$$\begin{aligned} \begin{Bmatrix} M_x \\ M_y \\ M_{xy} \end{Bmatrix} &= \begin{bmatrix} B_{11} & B_{12} & 0 \\ B_{12} & B_{22} & 0 \\ 0 & 0 & B_{66} \end{bmatrix} \begin{Bmatrix} \frac{\partial u_0}{\partial x} + \frac{1}{2}(\frac{\partial w_0}{\partial x})^2 \\ \frac{\partial v_0}{\partial y} + \frac{1}{2}(\frac{\partial w_0}{\partial y})^2 \\ \frac{\partial u_0}{\partial y} + \frac{\partial v_0}{\partial x} + \frac{\partial w_0}{\partial x}\frac{\partial w_0}{\partial y} \end{Bmatrix} \\ &\quad + \begin{bmatrix} D_{11} & D_{12} & 0 \\ D_{12} & D_{22} & 0 \\ 0 & 0 & D_{66} \end{bmatrix} \begin{Bmatrix} \frac{\partial \phi_x}{\partial x} \\ \frac{\partial \phi_y}{\partial y} \\ \frac{\partial \phi_x}{\partial y} + \frac{\partial \phi_y}{\partial x} \end{Bmatrix} \end{aligned} \tag{15}$$

$$\begin{Bmatrix} Q_x \\ Q_y \end{Bmatrix} = K\begin{bmatrix} A_{55} & 0 \\ 0 & A_{44} \end{bmatrix} \begin{Bmatrix} \frac{\partial w_0}{\partial x} + \phi_x \\ \frac{\partial w_0}{\partial y} + \phi_y \end{Bmatrix} \tag{16}$$

where

$$\begin{aligned} A_{11} &= \int_{-h/2}^{h/2} Q_{11}dz, \qquad A_{12} = \int_{-h/2}^{h/2} Q_{12}dz, \\ A_{22} &= \int_{-h/2}^{h/2} Q_{22}dz, \qquad A_{66} = \int_{-h/2}^{h/2} Q_{66}dz, \\ A_{44} &= \int_{-h/2}^{h/2} Q_{44}dz, \qquad A_{55} = \int_{-h/2}^{h/2} Q_{55}dz, \\ B_{11} &= \int_{-h/2}^{h/2} Q_{11}zdz, \qquad B_{12} = \int_{-h/2}^{h/2} Q_{12}zdz, \\ B_{22} &= \int_{-h/2}^{h/2} Q_{22}zdz, \qquad B_{66} = \int_{-h/2}^{h/2} Q_{66}zdz, \\ D_{11} &= \int_{-h/2}^{h/2} Q_{11}z^2dz, \qquad D_{12} = \int_{-h/2}^{h/2} Q_{12}z^2dz, \\ D_{22} &= \int_{-h/2}^{h/2} Q_{22}z^2dz, \qquad D_{66} = \int_{-h/2}^{h/2} Q_{66}z^2dz. \end{aligned} \tag{17}$$

The equations of motion Eq. (12) can be expressed in term of displacements $(u_0, v_0, w_0, \phi_x, \phi_y)$ by substituting Eqs. (14)–(16) into Eq. (12) as

$$A_{11}\left(\frac{\partial^2 u_0}{\partial x^2}+\frac{\partial^2 w_0}{\partial x}\frac{\partial^2 w_0}{\partial x^2}\right)+A_{12}\left(\frac{\partial^2 v_0}{\partial x\partial y}+\frac{\partial w_0}{\partial y}\frac{\partial^2 w_0}{\partial x\partial y}\right)+B_{11}\frac{\partial^2\phi_x}{\partial x^2}+B_{12}\frac{\partial^2\phi_y}{\partial x\partial y}+A_{66}\left(\frac{\partial^2 u_0}{\partial y^2}+\frac{\partial^2 v_0}{\partial x\partial y}+\frac{\partial^2 w_0}{\partial x\partial y}\frac{\partial w_0}{\partial y}+\frac{\partial w_0}{\partial x}\frac{\partial^2 w_0}{\partial y^2}\right)+B_{66}\left(\frac{\partial^2\phi_x}{\partial y^2}+\frac{\partial^2\phi_y}{\partial x\partial y}\right)=I_0\frac{\partial^2 u_0}{\partial t^2}+I_1\frac{\partial^2\phi_x}{\partial t^2} \tag{18a}$$

$$A_{12}\left(\frac{\partial^2 u_0}{\partial x\partial y}+\frac{\partial w_0}{\partial x}\frac{\partial^2 w_0}{\partial x\partial y}\right)+A_{22}\left(\frac{\partial^2 v_0}{\partial y^2}+\frac{\partial w_0}{\partial y}\frac{\partial^2 w_0}{\partial y^2}\right)+B_{12}\frac{\partial^2\phi_x}{\partial x\partial y}+B_{22}\frac{\partial^2\phi_y}{\partial y^2}+A_{66}\left(\frac{\partial^2 u_0}{\partial x\partial y}+\frac{\partial^2 v_0}{\partial x^2}+\frac{\partial^2 w_0}{\partial x^2}\frac{\partial w_0}{\partial y}+\frac{\partial w_0}{\partial x}\frac{\partial^2 w_0}{\partial x\partial y}\right)+B_{66}\left(\frac{\partial^2\phi_x}{\partial x\partial y}+\frac{\partial^2\phi_y}{\partial x^2}\right)=I_0\frac{\partial^2 v_0}{\partial t^2}+I_1\frac{\partial^2\phi_y}{\partial t^2} \tag{18b}$$

$$KA_{55}\left(\frac{\partial^2 w_0}{\partial x^2}+\frac{\partial\phi_x}{\partial x}\right)+KA_{44}\left(\frac{\partial^2 w_0}{\partial y^2}+\frac{\partial\phi_x}{\partial y}\right)+\frac{\partial}{\partial x}\left(\hat{N}_x\frac{\partial w_0}{\partial x}+\hat{N}_{xy}\frac{\partial w_0}{\partial y}\right)+\frac{\partial}{y}\left(\hat{N}_{xy}\frac{\partial w_0}{\partial x}+\hat{N}_y\frac{\partial w_0}{\partial y}\right)-K_1 w_0+K_2\left(\frac{\partial^2 w_0}{\partial x^2}+\frac{\partial^2 w_0}{\partial y^2}\right)+q=I_0\frac{\partial^2 w_0}{\partial t^2} \tag{18c}$$

$$B_{11}\left(\frac{\partial^2 u_0}{\partial x^2}+\frac{\partial w_0}{\partial x}\frac{\partial^2 w_0}{\partial x^2}\right)+B_{12}\left(\frac{\partial^2 v_0}{\partial x\partial y}+\frac{\partial w_0}{\partial y}\frac{\partial^2 w_0}{\partial x\partial y}\right)+D_{11}\frac{\partial^2\phi_x}{\partial x^2}+D_{12}\frac{\partial^2\phi_y}{\partial x\partial y}+B_{66}\left(\frac{\partial^2 u_0}{\partial y^2}+\frac{\partial^2 v_0}{\partial x\partial y}+\frac{\partial^2 w_0}{\partial x\partial y}\frac{\partial w_0}{\partial y}+\frac{\partial w_0}{\partial x}\frac{\partial^2 w_0}{\partial y^2}\right)+D_{66}\left(\frac{\partial^2\phi_x}{\partial y^2}+\frac{\partial^2\phi_y}{\partial x\partial y}\right)-KA_{55}\left(\frac{\partial w_0}{\partial x}+\phi_x\right)=I_1\frac{\partial^2 u_0}{\partial t^2}+I_2\frac{\partial^2\phi_x}{\partial t^2} \tag{18d}$$

$$B_{12}\left(\frac{\partial^2 u_0}{\partial x\partial y}+\frac{\partial w_0}{\partial x}\frac{\partial^2 w_0}{\partial x\partial y}\right)+B_{22}\left(\frac{\partial^2 v_0}{\partial y^2}+\frac{\partial w_0}{\partial y}\frac{\partial^2 w_0}{\partial y^2}\right)+D_{12}\frac{\partial^2\phi_x}{\partial x\partial y}+D_{22}\frac{\partial^2\phi_y}{\partial y^2}+B_{66}\left(\frac{\partial^2 u_0}{\partial x\partial y}+\frac{\partial^2 v_0}{\partial x^2}+\frac{\partial^2 w_0}{\partial x^2}\frac{\partial w_0}{\partial y}+\frac{\partial w_0}{\partial x}\frac{\partial^2 w_0}{\partial x\partial y}\right)+D_{66}\left(\frac{\partial^2\phi_x}{\partial x\partial y}+\frac{\partial^2\phi_y}{\partial x^2}\right)-KA_{44}\left(\frac{\partial w_0}{\partial y}+\phi_y\right)=I_1\frac{\partial^2 v_0}{\partial t^2}+I_2\frac{\partial^2\phi_y}{\partial t^2} \tag{18e}$$

To discuss the Navier solution, the equations of motion (18) can be written as

$$\frac{\partial}{\partial x}\left[A_{11}\frac{\partial u_0}{\partial x}+A_{12}\frac{\partial v_0}{\partial y}+B_{11}\frac{\partial\phi_x}{\partial x}+B_{12}\frac{\partial\phi_y}{\partial y}\right]+\frac{\partial}{\partial y}\left[A_{66}\left(\frac{\partial u_0}{\partial y}+\frac{\partial v_0}{\partial x}\right)+B_{66}\left(\frac{\partial\phi_x}{\partial y}+\frac{\partial\phi_y}{\partial x}\right)\right]=I_0\frac{\partial^2 u_0}{\partial t^2}+I_1\frac{\partial^2\phi_x}{\partial t^2} \tag{19a}$$

$$\frac{\partial}{\partial x}\left[A_{66}\left(\frac{\partial u_0}{\partial y}+\frac{\partial v_0}{\partial x}\right)+B_{66}\left(\frac{\partial\phi_x}{\partial y}+\frac{\partial\phi_y}{\partial x}\right)\right]+\frac{\partial}{\partial y}\left[A_{12}\frac{\partial u_0}{\partial x}+A_{22}\frac{\partial v_0}{\partial y}+B_{12}\frac{\partial\phi_x}{\partial x}+B_{22}\frac{\partial\phi_y}{\partial y}\right]=I_0\frac{\partial^2 v_0}{\partial t^2}+I_1\frac{\partial^2\phi_y}{\partial t^2} \tag{19b}$$

$$\frac{\partial}{\partial x}\left[KA_{55}\left(\frac{\partial w_0}{\partial x}+\phi_x\right)\right]+\frac{\partial}{\partial y}\left[KA_{44}\left(\frac{\partial w_0}{\partial y}+\phi_y\right)\right]+\hat{N}_x\frac{\partial^2 w_0}{\partial x^2}+2\hat{N}_{xy}\frac{\partial^2 w_0}{\partial y\partial x}+\hat{N}_y\frac{\partial^2 w_0}{\partial y^2}-K_1 w_0+K_2\left(\frac{\partial^2 w_0}{\partial x^2}+\frac{\partial^2 w_0}{\partial y^2}\right)+q=I_0\frac{\partial^2 w_0}{\partial t^2} \tag{19c}$$

$$\frac{\partial}{\partial x}\left[B_{11}\frac{\partial u_0}{\partial x}+B_{12}\frac{\partial v_0}{\partial y}+D_{11}\frac{\partial\phi_x}{\partial x}+D_{12}\frac{\partial\phi_y}{\partial y}\right]+\frac{\partial}{\partial y}\left[B_{66}\left(\frac{\partial u_0}{\partial y}+\frac{\partial v_0}{\partial x}\right)+D_{66}\left(\frac{\partial\phi_x}{\partial y}+\frac{\partial\phi_y}{\partial x}\right)\right]-KA_{55}\left(\frac{\partial w_0}{\partial x}+\phi_x\right)=I_1\frac{\partial^2 u_0}{\partial t^2}+I_2\frac{\partial^2\phi_x}{\partial t^2} \tag{19d}$$

$$\frac{\partial}{\partial x}\left[B_{66}\left(\frac{\partial u_0}{\partial y}+\frac{\partial v_0}{\partial x}\right)+D_{66}\left(\frac{\partial\phi_x}{\partial y}+\frac{\partial\phi_y}{\partial y}\right)\right]+\frac{\partial}{\partial y}\left[B_{12}\frac{\partial u_0}{\partial x}+B_{22}\frac{\partial v_0}{\partial y}+D_{12}\frac{\partial\phi_x}{\partial x}+D_{22}\frac{\partial\phi_y}{\partial y}\right]+-KA_{44}\left(\frac{\partial w_0}{\partial y}+\phi_y\right)=I_1\frac{\partial^2 v_0}{\partial t^2}+I_2\frac{\partial^2\phi_y}{\partial t^2} \tag{19e}$$

3. Boundary condition and Navier solution

According to the FSDT, the simply supported boundary conditions for the FG-CNTRC plate are

$$\begin{aligned}
&u_0(x,0,t)=0, && u_0(x,b,t)=0,\\
&v_0(0,y,t)=0, && v_0(a,y,t)=0\\
&w_0(x,0,t)=0, && w_0(x,b,t)=0,\\
&w_0(0,y,t)=0, && w_0(a,y,t)=0\\
&\phi_x(x,0,t)=0, && \phi_x(x,b,t)=0,\\
&\phi_y(0,y,t)=0, && \phi_y(a,y,t)=0
\end{aligned} \tag{20a}$$

$$\begin{aligned}
&N_x(0,y,t)=0, && N_x(a,y,t)=0,\\
&N_y(x,0,t)=0, && N_y(x,b,t)=0\\
&M_x(0,y,t)=0, && M_x(a,y,t)=0,\\
&M_y(x,0,t)=0, && M_y(x,b,t)=0
\end{aligned} \tag{20b}$$

The boundary conditions in Eq. (20) are satisfied by the following expansions

$$u_0(x,y,t)=\sum_{n=1}^{\infty}\sum_{m=1}^{\infty}U_{mn}(t)\cos(\alpha x)\sin(\beta x) \tag{21}$$

$$v_0(x,y,t)=\sum_{n=1}^{\infty}\sum_{m=1}^{\infty}V_{mn}(t)\sin(\alpha x)\cos(\beta x) \tag{22}$$

$$w_0(x,y,t)=\sum_{n=1}^{\infty}\sum_{m=1}^{\infty}W_{mn}(t)\sin(\alpha x)\sin(\beta x) \tag{23}$$

$$\phi_x(x,y,t)=\sum_{n=1}^{\infty}\sum_{m=1}^{\infty}X_{mn}(t)\cos(\alpha x)\sin(\beta x) \tag{24}$$

$$\phi_y(x,y,t) = \sum_{n=1}^{\infty}\sum_{m=1}^{\infty} Y_{mn}(t)\sin(\alpha x)\cos(\beta x) \tag{25}$$

where $\alpha = m\pi/a$ and $\alpha = n\pi/b$.

For the mechanical load, $q(x,y,t)$ is also expanded in double Fourier sine series as follows:

$$q(x,y,t) = \sum_{n=1}^{\infty}\sum_{m=1}^{\infty} Q_{mn}(t)\sin(\alpha x)\sin(\beta y). \tag{26}$$

The coefficients Q_{mn} for the case of uniformly distributed load (UDL) are defined as follows:

$$Q_{mn} = \begin{cases} \frac{16q_0}{mn\pi^2} & \text{for } m,n, \text{ old,} \\ 0 & \text{for } m,n, \text{ even,} \end{cases} \tag{27}$$

where q_0 represents the intensity of the load at the plate.

Substitution of Eqs. (21)–(26) into Eq. (19) will show that the Navier solution as

$$\begin{bmatrix} C_{11} & C_{12} & 0 & C_{14} & C_{15} \\ C_{12} & C_{22} & 0 & C_{15} & C_{25} \\ 0 & 0 & C_{33} & C_{34} & C_{35} \\ C_{14} & C_{15} & C_{34} & C_{44} & C_{45} \\ C_{15} & C_{25} & C_{35} & C_{45} & C_{55} \end{bmatrix} \begin{Bmatrix} U_{mn} \\ V_{mn} \\ W_{mn} \\ X_{mn} \\ Y_{mn} \end{Bmatrix} + \begin{bmatrix} m_{11} & 0 & 0 & 0 & 0 \\ 0 & m_{22} & 0 & 0 & 0 \\ 0 & 0 & m_{33} & 0 & 0 \\ 0 & 0 & 0 & m_{44} & 0 \\ 0 & 0 & 0 & 0 & m_{55} \end{bmatrix} \begin{Bmatrix} \ddot{U}_{mn} \\ \ddot{V}_{mn} \\ \ddot{W}_{mn} \\ \ddot{X}_{mn} \\ \ddot{Y}_{mn} \end{Bmatrix} = \begin{Bmatrix} 0 \\ 0 \\ Q_{mn} \\ 0 \\ 0 \end{Bmatrix} \tag{28}$$

where

$$\begin{aligned} C_{11} &= A_{11}\alpha^2 + A_{66}\beta^2, \qquad C_{12} = (A_{12} + A_{66})\alpha\beta, \\ C_{14} &= B_{11}\alpha^2 + B_{66}\beta^2, \qquad C_{15} = (B_{12} + B_{66})\alpha\beta, \\ C_{22} &= A_{22}\beta^2 + A_{66}\alpha^2, \qquad C_{25} = B_{22}\beta^2 + B_{66}\alpha^2, \\ C_{33} &= KA_{55}\alpha^2 + KA_{44}\beta^2 + \hat{N}_x\alpha^2 + \hat{N}_y\beta^2 + K_1 + K_2\left(\alpha^2+\beta^2\right) \\ C_{34} &= KA_{55}\alpha, \qquad C_{35} = KA_{44}\beta \\ C_{44} &= \left(D_{11}\alpha^2 + D_{66}\beta^2 + KA_{55}\right), \\ C_{45} &= (D_{12} + D_{66})\alpha\beta, \qquad C_{55} = \left(D_{22}\beta^2 + D_{66}\alpha^2 + KA_{44}\right), \\ m_{11} &= m_{22} = m_{33} = I_0, \qquad m_{44} = m_{55} = I_2 \end{aligned} \tag{29}$$

4. Static response and free vibration analyses

4.1. Static response analysis

The static response can be obtained from Eq. (28) by setting the time derivative terms and edge forces to zero:

$$\begin{bmatrix} C_{11} & C_{12} & 0 & C_{14} & C_{15} \\ C_{12} & C_{22} & 0 & C_{15} & C_{25} \\ 0 & 0 & C^*_{33} & C_{34} & C_{35} \\ C_{14} & C_{15} & C_{34} & C_{44} & C_{45} \\ C_{15} & C_{25} & C_{35} & C_{45} & C_{55} \end{bmatrix} \begin{Bmatrix} U_{mn} \\ V_{mn} \\ W_{mn} \\ X_{mn} \\ Y_{mn} \end{Bmatrix} = \begin{Bmatrix} 0 \\ 0 \\ Q_{mn} \\ 0 \\ 0 \end{Bmatrix} \tag{30}$$

where $C^*_{33} = KA_{55}\alpha^2 + KA_{44}\beta^2 + K_1 + K_2(\alpha^2+\beta^2)$.

Solution of Eq. (30) for each $m,n = 1,2,3,\ldots$ gives $(U_{mn}, V_{mn}, W_{mn}, X_{mn}, Y_{mn})$, which can then be used to compute the solution $(u_0, v_0, w_0, \phi_x, \phi_y)$ from Eqs. (21)–(25).

Let us consider three cases (UD, FG-O, FG-X), $B_{ij} = 0$. Consequently, $C_{14} = 0$, $C_{15} = 0$ and $C_{25} = 0$. From Eq. (30), (U_{mn}, V_{mn}) are uncoupled from (W_{mn}, X_{mn}, Y_{mn}):

$$\begin{bmatrix} C_{11} & C_{12} & 0 & 0 & 0 \\ C_{12} & C_{22} & 0 & 0 & 0 \\ 0 & 0 & C^*_{33} & C_{34} & C_{35} \\ 0 & 0 & C_{34} & C_{44} & C_{45} \\ 0 & 0 & C_{35} & C_{45} & C_{55} \end{bmatrix} \begin{Bmatrix} U_{mn} \\ V_{mn} \\ W_{mn} \\ X_{mn} \\ Y_{mn} \end{Bmatrix} = \begin{Bmatrix} 0 \\ 0 \\ Q_{mn} \\ 0 \\ 0 \end{Bmatrix} \tag{31}$$

Decoupling the in-plane displacements from the bending displacements, so

$$\begin{bmatrix} C_{11} & C_{12} \\ C_{12} & C_{22} \end{bmatrix} \begin{Bmatrix} U_{mn} \\ V_{mn} \end{Bmatrix} = \begin{Bmatrix} 0 \\ 0 \end{Bmatrix} \tag{32}$$

$$\begin{bmatrix} C^*_{33} & C_{34} & C_{35} \\ C_{34} & C_{44} & C_{45} \\ C_{35} & C_{45} & C_{55} \end{bmatrix} \begin{Bmatrix} W_{mn} \\ X_{mn} \\ Y_{mn} \end{Bmatrix} = \begin{Bmatrix} Q_{mn} \\ 0 \\ 0 \end{Bmatrix} \tag{33}$$

In Eq. (32) the in-plane deflections are identically zero when the forces are zero. From Eq. (33), the coefficients (W_{mn}, X_{mn}, Y_{mn}) can be determined as:

$$\begin{aligned} W_{mn} &= \frac{Q_{mn}(C_{44}C_{55} - C_{45}C_{45})}{C_{33}(C_{44}C_{55} - C_{45}C_{45}) + C_{34}(C_{45}C_{35} - C_{34}C_{55}) + C_{35}(C_{34}C_{45} - C_{44}C_{35})} \\ X_{mn} &= \frac{Q_{mn}(C_{45}C_{35} - C_{34}C_{55})}{C_{33}(C_{44}C_{55} - C_{45}C_{45}) + C_{34}(C_{45}C_{35} - C_{34}C_{55}) + C_{35}(C_{34}C_{45} - C_{44}C_{35})} \\ Y_{mn} &= \frac{Q_{mn}(C_{44}C_{45} - C_{44}C_{35})}{C_{33}(C_{44}C_{55} - C_{45}C_{45}) + C_{34}(C_{45}C_{35} - C_{34}C_{55}) + C_{35}(C_{34}C_{45} - C_{44}C_{35})} \end{aligned} \tag{34}$$

4.2. Natural vibration analysis

For free vibration problem, we set the mechanical load to zero, and we assume a periodic solution of the form:

$$\begin{aligned} U_{mn}(t) &= U^0_{mn}e^{i\omega t} \\ V_{mn}(t) &= V^0_{mn}e^{i\omega t} \\ W_{mn}(t) &= W^0_{mn}e^{i\omega t} \\ X_{mn}(t) &= X^0_{mn}e^{i\omega t} \\ Y_{mn}(t) &= Y^0_{mn}e^{i\omega t} \end{aligned} \tag{35}$$

where $i = \sqrt{-1}$ and ω is the frequency of natural vibration. Substitution of Eq. (35) into Eq. (28) as

$$\left(\begin{bmatrix} C_{11} & C_{12} & 0 & C_{14} & C_{15} \\ C_{12} & C_{22} & 0 & C_{15} & C_{25} \\ 0 & 0 & C^*_{33} & C_{34} & C_{35} \\ C_{14} & C_{15} & C_{34} & C_{44} & C_{45} \\ C_{15} & C_{25} & C_{35} & C_{45} & C_{55} \end{bmatrix} - \omega^2 \begin{bmatrix} \tilde{C}_{11} & 0 & 0 & 0 & 0 \\ 0 & \tilde{C}_{22} & 0 & 0 & 0 \\ 0 & 0 & \tilde{C}_{33} & 0 & 0 \\ 0 & 0 & 0 & \tilde{C}_{44} & 0 \\ 0 & 0 & 0 & 0 & \tilde{C}_{55} \end{bmatrix}\right) \begin{Bmatrix} U^0_{mn} \\ V^0_{mn} \\ W^0_{mn} \\ X^0_{mn} \\ Y^0_{mn} \end{Bmatrix} = \begin{Bmatrix} 0 \\ 0 \\ 0 \\ 0 \\ 0 \end{Bmatrix} \tag{36}$$

When rotary is omitted, Eq. (36) can be simplified by eliminating. We obtain the following 3×3 system of eigenvalue problem

$$\left(\begin{bmatrix} \hat{C}_{11} & \hat{C}_{12} & \hat{C}_{13} \\ \hat{C}_{12} & \hat{C}_{22} & \hat{C}_{23} \\ \hat{C}_{13} & \hat{C}_{21} & \hat{C}_{33} \end{bmatrix} - \omega^2 \begin{bmatrix} \hat{C}_{11} & 0 & 0 \\ 0 & \hat{C}_{22} & 0 \\ 0 & 0 & \hat{C}_{33} \end{bmatrix}\right) \begin{Bmatrix} U^0_{mn} \\ V^0_{mn} \\ W^0_{mn} \end{Bmatrix} = \begin{Bmatrix} 0 \\ 0 \\ 0 \end{Bmatrix} \tag{37}$$

where

$$\hat{C}_{11} = C_{11} - \frac{(C_{14}C_{55} - C_{15}C_{45})C_{14}}{C_{44}C_{55} - C_{45}^2} - \frac{(C_{15}C_{44} - C_{14}C_{45})C_{15}}{C_{44}C_{55} - C_{45}^2}$$
$$\hat{C}_{12} = C_{12} - \frac{(C_{15}C_{55} - C_{25}C_{45})C_{14}}{C_{44}C_{55} - C_{45}^2} - \frac{(C_{25}C_{44} - C_{15}C_{45})C_{15}}{C_{44}C_{55} - C_{45}^2}$$
$$\hat{C}_{13} = -\frac{(C_{34}C_{55} - C_{35}C_{45})C_{14}}{C_{44}C_{55} - C_{45}^2} - \frac{(C_{35}C_{44} - C_{34}C_{45})C_{15}}{C_{44}C_{55} - C_{45}^2}$$
$$\hat{C}_{22} = C_{22} - \frac{(C_{15}C_{55} - C_{25}C_{45})C_{15}}{C_{44}C_{55} - C_{45}^2} - \frac{(C_{25}C_{44} - C_{15}C_{45})C_{25}}{C_{44}C_{55} - C_{45}^2} \quad (38)$$
$$\hat{C}_{23} = \frac{(C_{35}C_{55} - C_{35}C_{45})C_{15}}{C_{44}C_{55} - C_{45}^2} - \frac{(C_{35}C_{44} - C_{35}C_{45})C_{25}}{C_{44}C_{55} - C_{45}^2}$$
$$\hat{C}_{33} = C_{33}^* - \frac{(C_{34}C_{55} - C_{35}C_{45})C_{34}}{C_{44}C_{55} - C_{45}^2} - \frac{(C_{35}C_{44} - C_{34}C_{45})C_{35}}{C_{44}C_{55} - C_{45}^2}$$

If the in-plane and rotary inertias are omitted (i.e., $m_{11} = m_{22} = m_{44} = m_{55} = 0$), we have

$$\omega^2 = \left(\hat{C}_{33} - \frac{\hat{C}_{22}\hat{C}_{13}^2 - \hat{C}_{23}\hat{C}_{12}\hat{C}_{13}}{\hat{C}_{11}\hat{C}_{22} - \hat{C}_{33}\hat{C}_{13}^2} - \frac{\hat{C}_{11}\hat{C}_{23}^2 - \hat{C}_{12}\hat{C}_{13}\hat{C}_{23}}{\hat{C}_{11}\hat{C}_{22} - \hat{C}_{33}\hat{C}_{13}^2}\right)\frac{1}{m_{33}} \quad (39)$$

5. Numerical results

In this section, several numerical examples are presented to study the static response and free vibration of CNTRC plates. Poly{(m-phenylenevinylene)-co-[(2,5-dioctoxy-p-phe-nylene)vinylene]} (PmPV) is considered as the matrix and the mean material properties are assumed to be $\nu_m = 0.34$, $\rho_m = 1150$ kg/m^3 and $E_m = 2.1$ GPa (at room temperature 300 K). And the armchair (10, 10) SWCNTs are selected as the reinforcements. Based on the results of Ref. [45], the material properties of SWCNTs are given by $E_{11}^{CNT} = 5.6466$ (TPa), $E_{22}^{CNT} = 7.08$ (TPa) and $G_{12}^{CNT} = 31.9445$ (TPa). The CNT efficiency parameter shown in Ref. [44], for example: $\eta_1 = 0.149$, $\eta_2 = 0.934$ for the case $V_{CNT}^* = 0.11$. and $\eta_1 = 0.137$, $\eta_2 = 1.022$ for the case $V_{CNT}^* = 0.12$, and $\eta_1 = 0.142$, $\eta_2 = 1.626$ for the case $V_{CNT}^* = 0.17$, and $\eta_1 = 0.141$, $\eta_2 = 1.585$ for the case $V_{CNT}^* = 0.28$. Note that $\eta_3 = \eta_2$ and $G_{23} = G_{13} = G_{12}$.

The dimensionless quantities of the elastic foundation parameters can be defined as follows:

$$k_1 = K_1\frac{b^4}{E_m h^3}, \qquad k_2 = K_2\frac{b^2}{E_m h^3} \quad (40)$$

5.1. Comparison studies

In order to validate the results of present formulation, several comparison studies are carried out in Tables 1–3. Firstly, Table 1 shows the comparison of the non-dimensional central deflection, $\bar{w} = -w_0/h$ for the simply supported FG-CNTRC plate subjected to a uniform load without elastic foundations ($a = b$, $V_{CNT}^* = 11\%$). In this table, the present formulation method is compared with those reported by Phung-Van et al. [33] and Zhu et al. [50]. Three types of distributions of carbon nanotubes along the thickness direction are considered: UD, FG-O and FG-X. The calculations for the first-order shear deformation theory, the shear correction factor K is selected to be 5/6. Noted that the results presented in Ref. [33] are based on the isogeometric analysis, in Ref. [50] are based on the finite element method while the results of this study are obtained by an exact solution. It is concluded from Table 1 that the results agree well with the previous work in Refs. [33,50].

Table 1
The comparison of the non-dimensional central deflection, $\bar{w} = -w_0/h$ for the simply supported FG-CNTRC plate subjected to the uniform load without elastic foundations ($a = b$, $V_{CNT}^* = 11\%$).

h/a	Types	Method		
		Present	Ref. [33] (IGA)	Ref. [50] (FEM)
0.02	UD	1.2853	1.1630	1.1550
	FG-O	2.3403	2.2001	2.1570
	FG-X	0.8947	0.7877	0.7900
0.05	UD	3.9077E−02	3.546E−02	3.628E−02
	FG-O	6.5691E−02	6.170E−02	6.155E−02
	FG-X	2.9179E−02	2.591E−02	2.701E−02

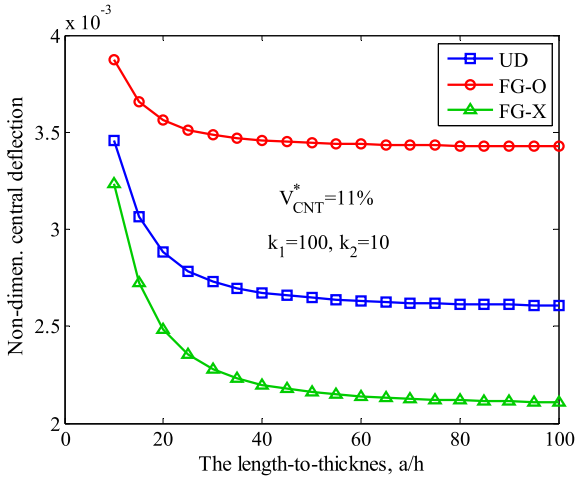

Fig. 2. Non-dimensional central deflection versus length-to-thickness ratio for simply supported CNTRC plates under the distributed load ($q_0 = -1.0 \times 10^5$ N/m^2).

Using Eq. (39), the non-dimensional frequency parameter obtained as:

$$\bar{\omega} = \omega\frac{b^2}{\pi^2}\sqrt{\frac{\rho_m h}{D}} \quad (41)$$

where $D = E_m h^3/[12(1 - \nu_m^2)]$.

Next, in order to verify the results of free vibration analysis, the non-dimensional frequency parameter, $\omega(b^2/\pi^2)\sqrt{\rho_m h/D}$ of various types of FG-CNTRC plates in different thickness-to-width ratio, h/b with SSSS boundary conditions are examined and compared with results of Zhang et al. [51] using the element-free IMLS-Ritz method as in Table 2. Table 2 clearly shows that the present frequency parameter agree very well with the solutions of Zhang et al. [51].

Finally, Table 3 also presents the comparison of non-dimensional frequency parameter, $\omega(a^2/h)\sqrt{\rho_m/E_m}$ of various types of simply supported FG-CNTRC plates without elastic foundations with those reported by Phung-Van et al. [33] and Zhu et al. [50]. It can be found that the solutions obtained using the exact solution are in good agreement.

5.2. Results for statics response of FG-CNTRC plates

After validating the present approach, the parametric studies are presented in this subsection. The following non-dimensional central deflection of the plate can be defined as:

$$\bar{w} = w_0\left(\frac{E_m h^3}{b^4 q_0}\right) \quad (42)$$

Fig. 2 shows the variation of non-dimensional central deflection versus length-to-thickness ratio for simply supported FG-CNTRC

Table 2
Comparison of non-dimensional frequency parameter, $\bar{\omega} = \omega(b^2/\pi^2)\sqrt{\rho_m h/D}$ of various types of CNTRC plates in different thickness-to-width ratio, h/b with SSSS boundary conditions.

Types	Fundamental frequency parameter							
	$h/b = 0.001$		$h/b = 0.01$		$h/b = 0.05$		$h/b = 0.1$	
	Present	Ref. [51]	Present	Ref. [51]	Present	Ref. [51]	Present	Ref. [51]
UD	5.86764	5.9474	5.83291	5.817	5.14924	5.0186	3.99244	3.76339
	1.34%		0.27%		2.60%		6.10%	
FG-O	4.29001	4.4434	4.27730	4.2941	4.0005	3.9569	3.40736	3.2737
	3.4%		0.17%		1.1%		4.1%	
FG-V	4.91410	5.0427	4.89444	4.8945	4.48367	4.4028	3.68007	3.5031
	2.60%		0.02%		1.80%		5.10%	
FG-X	7.10547	7.1718	7.04322	7.0045	5.91457	5.7135	4.31029	4.0241
	0.92%		0.60%		3.50%		7.10%	

Table 3
The comparison of non-dimensional frequency parameter, $\omega(a^2/h)\sqrt{\rho_m/E_m}$ of various types of simply supported CNTRC plates without elastic foundations.

h/a	Mode (m,n)	FG-V			FG-O			FG-X		
		Present	Ref. [33] (IGA)	Ref. [50] (FEM)	Present	Ref. [33] (IGA)	Ref. [50] (FEM)	Present	Ref. [33] (IGA)	Ref. [50] (FEM)
10	(1, 1)	11.732	12.755	12.542	10.779	12.254	11.55	14.064	15.254	14.616
	(1, 2)	16.239	17.128	17.060	15.347	18.825	16.265	18.080	18.825	18.646
	(2, 1)	30.590	27.158	23.340	29.295	28.004	26.513	30.591	28.004	28.519
	(2, 2)	32.900	33.227	31.417	31.594	35.980	30.280	32.900	35.980	33.598
20	(1, 1)	13.855	15.127	15.110	12.316	13.500	13.523	18.571	20.241	19.939
	(1, 2)	18.270	19.606	16.903	16.560	18.371	18.486	22.142	23.573	23.776
	(2, 1)	45.004	38.855	38.998	41.121	38.855	38.998	54.676	38.855	38.998
	(2, 2)	46.929	48.298	47.739	43.116	44.759	43.948	56.258	49.581	52.689
50	(1, 1)	14.716	16.093	16.252	12.895	14.153	14.302	20.959	22.88	22.984
	(1, 2)	19.083	20.683	21.142	17.423	19.154	19.373	24.338	26.183	26.784
	(2, 1)	55.001	59.872	60.188	48.301	52.616	53.035	76.629	53.604	83.150
	(2, 2)	56.816	62.118	62.780	50.214	55.123	55.823	77.944	83.703	84.896

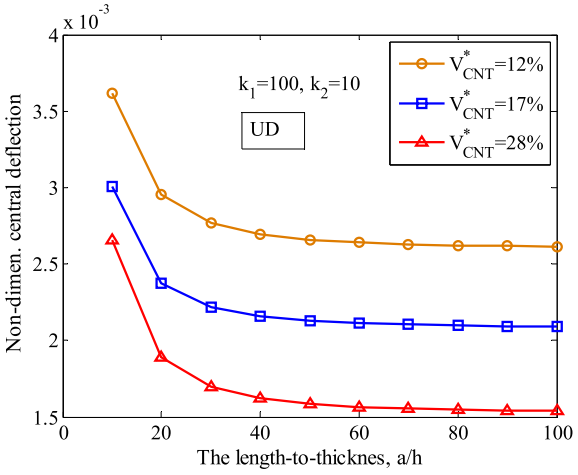

Fig. 3. Non-dimensional central deflection versus length-to-thickness ratio for simply supported CNTRC plates under distributed load for UD profile ($q_0 = -1.0 \times 10^5$ N/m^2).

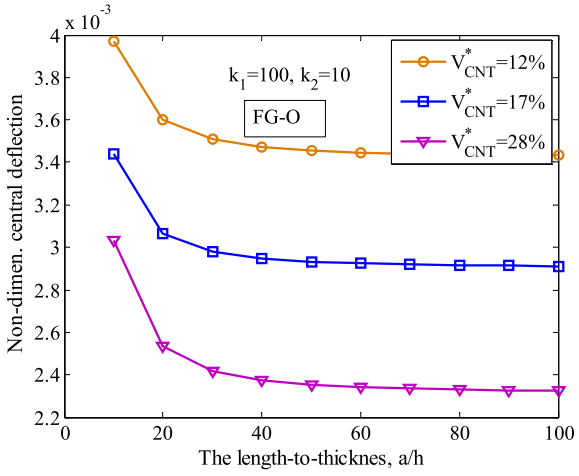

Fig. 4. Non-dimensional central deflection versus length-to-thickness ratio for simply supported CNTRC plates under distributed load for FG-O profile ($q_0 = -1.0 \times 10^5$ N/m^2).

plates under distributed load ($q_0 = -1.0 \times 10^5$ N/m^2) for the case of UD, FG-O and FG-X, respectively. The volume fraction of CNT is assumed to be 11%. In this case, the length-to-thickness ratio varies from $a/h = 10$ to $a/h = 100$. It is noteworthy that the CNT distribution of plate makes to effect of center deflection. Moreover, it can be seen that the non-dimensional central deflection of FG-X plate has lowest, while the FG-O plate has higher deflection, and that the central deflection of the UD plate lies between FG-X and FG-O.

Figs. 3–5 present the influence of CNT volume fraction V^*_{CNT} on non-dimensional central deflection versus length-to-thickness for three cases of CNT distribution UD, FG-O, and FG-X, respectively. For these example, the stiffnesses are $(k_1, k_2) = (100, 10)$ for the Winkler–Pasternak foundation. Three types of CNT volume fraction V^*_{CNT} are taken to be 12%, 17% and 28%. From figures, it is observed that the central deflection decreases when CNT volume fraction increases.

5.3. Results for free vibration analysis of FG-CNTRC plates

In order to investigate the free vibration problem of FG-CNTTC plates, the non-dimensional frequency parameters of the plate can be determined as:

$$\omega_n = \omega \frac{a^2}{h}\sqrt{\frac{\rho_m}{E_m}} \tag{43}$$

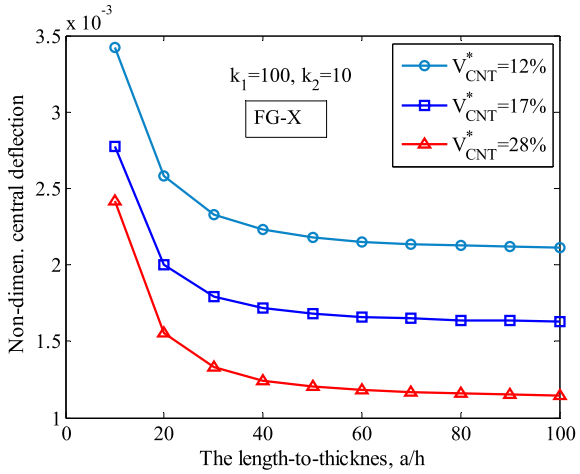

Fig. 5. Non-dimensional central deflection versus length-to-thickness ratio for simply supported CNTRC plates under distributed load for FG-X profile ($q_0 = -1.0 \times 10^5$ N/m^2).

As a first example, the effects of thickness-to-width ratio (h/b) together with the different CNTs distributions $(UD, FG-O, FG-V, FG-X)$ on the fundamental frequency parameter ω_n of FG-CNTRC plates with the different volume fraction of CNTs are presented in Fig. 6. The parameters of elastic foundation are taken to be $k_1 = 100$ and $k_2 = 10$. It can be found that for all types of the CNTs distributions, the fundamental frequency parameters decrease approximately to 20. As it can be observed that the FG-CNTRC plate with FG-X distributions has highest fundamental frequency. Moreover, it can be seen that fundamental frequency parameters are significantly affected by the ratio (h/b). In the first stage when the aspect ratio (h/b) is small, there is a big difference in fundamental frequency parameter of four types of CNT distribution but when h/b ratio increases further from 0.1 to 0.2, the change is small between all the types.

The variation of the first non-dimensional frequency parameter $\omega_n = \omega^2\sqrt{\rho_m/E_m}/h$ of FG-CNTRC plate resting on Winkler–Pasternak foundation ($k_1 = 100$, $k_2 = 10$) versus the thickness-width ratio (h/b) with the different volume fraction of CNTs is shown in Fig. 7. Geometrical parameter of FG-CNTRC plate is taken to be $a/b = 1.25$. Three different values of CNT volume fraction are considered as $V^*_{CNT} = 12\%$, $V^*_{CNT} = 17\%$ and $V^*_{CNT} = 28\%$. It can be also seen that the FG-CNTRC plate has higher fundamental frequency with the volume fraction changes from 12% to 28%.

Fig. 8 shows the influence of the Winkler modulus parameter (k_1) on the first fundamental frequency parameters of the FG-CNTRC for the four types of CNTs distributions $(UD, FG-O, FG-V, FG-X)$ together with the different volume fraction of CNTs, V^*_{CNT} $(= 11\%, 12\%, 17\%, 28\%)$. The geometrical parameters of the FG-CNTRC plate are selected as: $a/b = 1.25$, $b/h = 20$. As expected, the fundamental frequency is increased with increase in foundation stiffness for all types of CNTs distributions. Moreover, plates with FG-X and FG-O of CNTs distributions have the greatest and the smallest values of the fundamental frequency parameters, respectively.

The effects of the length-to-width ratio (a/b) on the non-dimensional fundamental frequency parameter of the FG-CNTRC plates with various the Winkler foundation parameter ranging from 0 to 1000 are plotted in Fig. 9. It is clear that for all type of CNT distributions, by increasing ratio a/b, the fundamental frequency parameter increases. Moreover, the trend of variations of

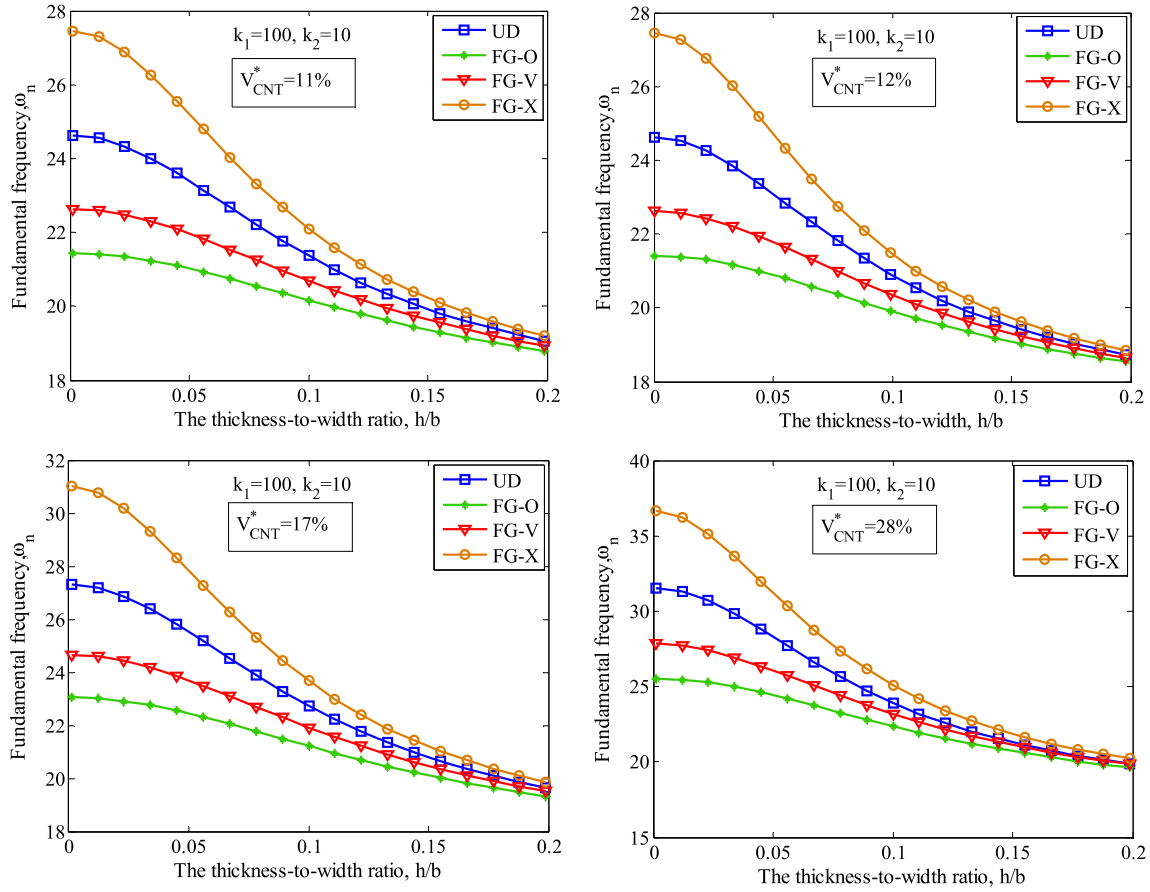

Fig. 6. Effect of thickness-to-width ratio h/b on the fundamental frequency parameter of the CNTRC plates for various types of CNTs distributions.

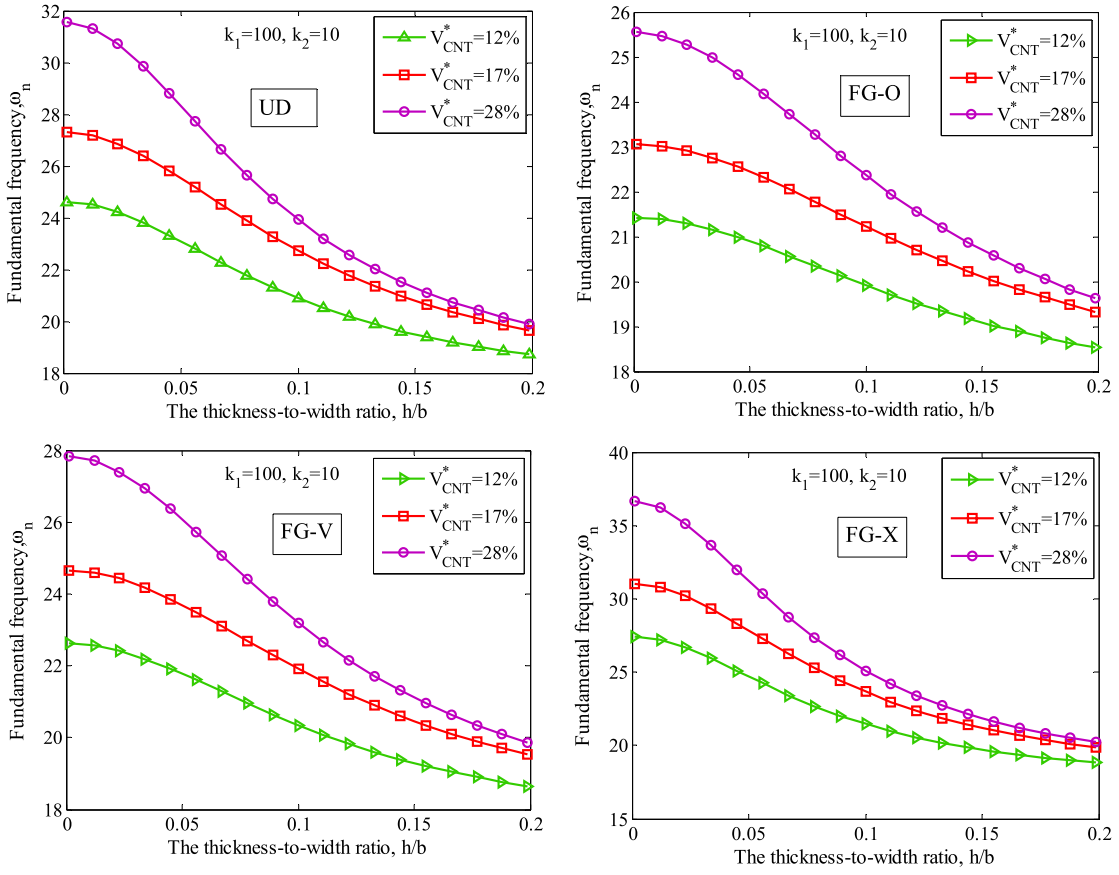

Fig. 7. Effect of thickness-to-width ratio h/b on the fundamental frequency parameter of various of CNTRC plates various values of V^*_{CNT}.

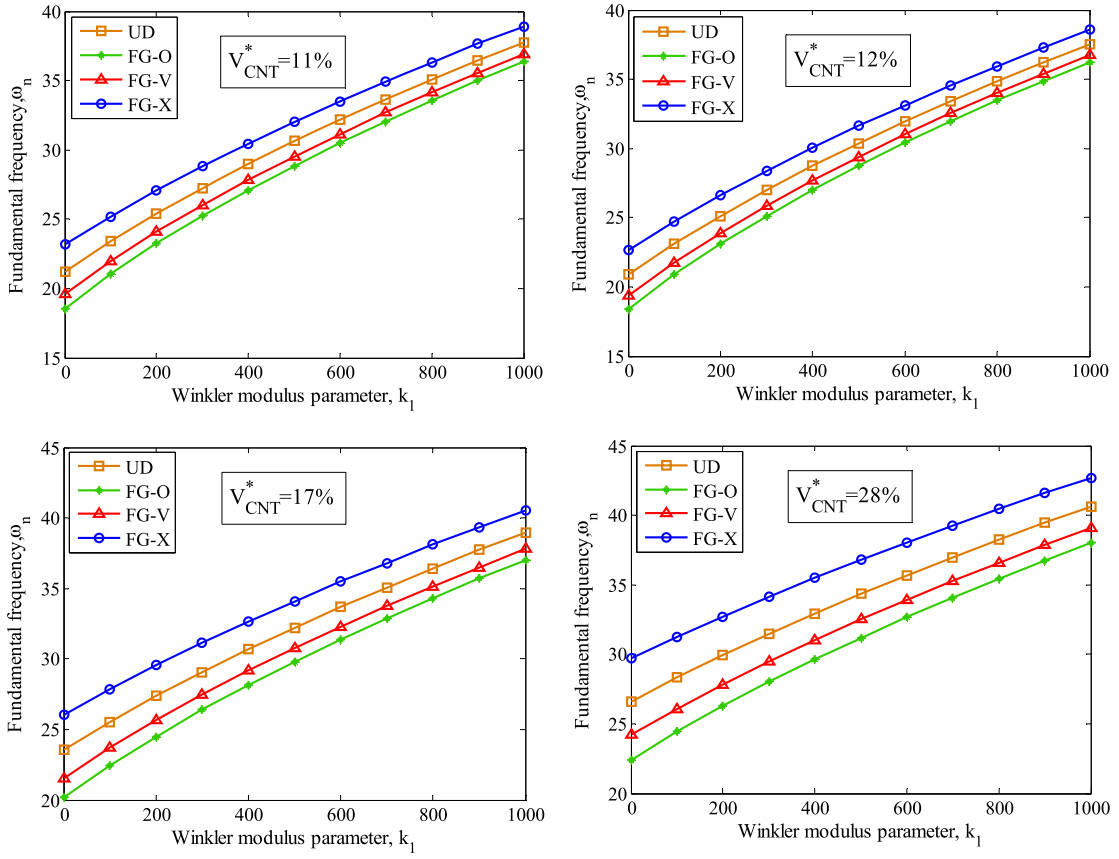

Fig. 8. Effect of the Winkler modulus parameter k_1 on the fundamental frequency parameter of various of CNTRC plates ($b/h = 20$, $a/b = 1$).

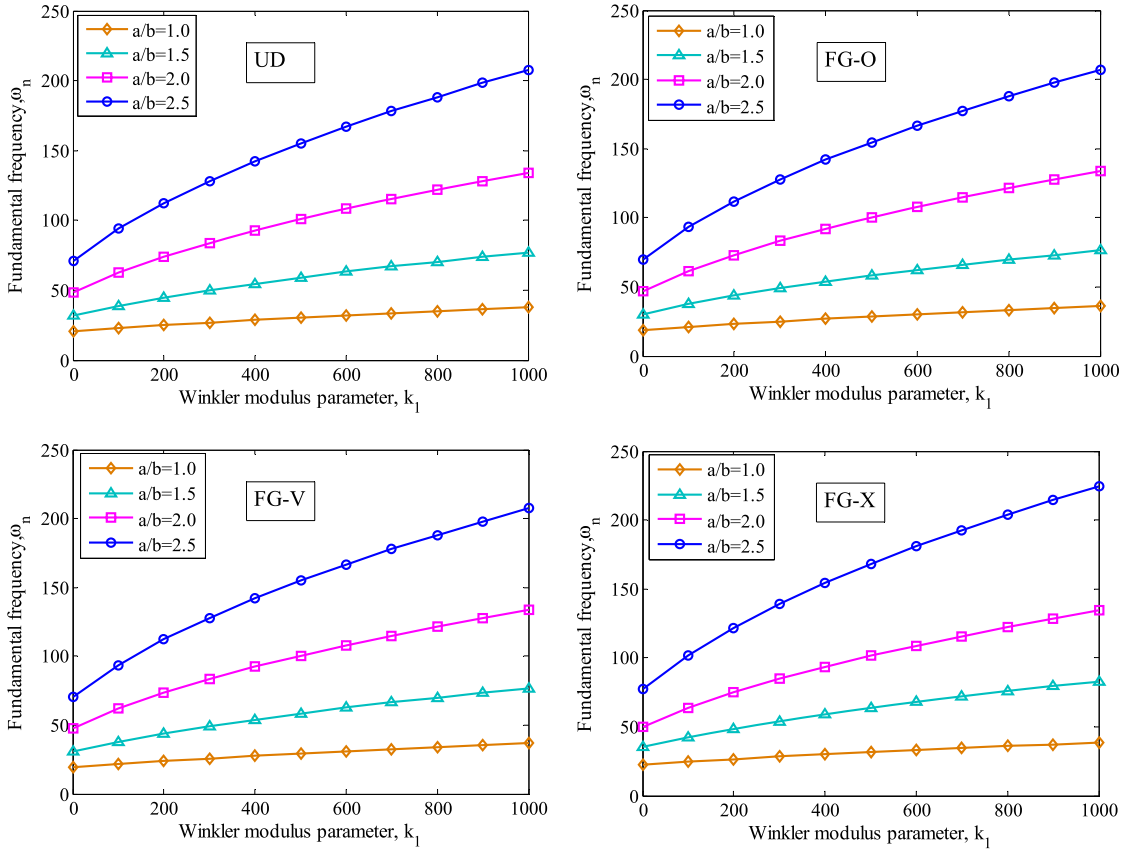

Fig. 9. Effect of the Winkler modulus parameter on the fundamental frequency parameter of the CNTRC plates for various values of a/b ratio ($b/h = 20$, $V^*_{CNT} = 12\%$, $k_2 = 10$).

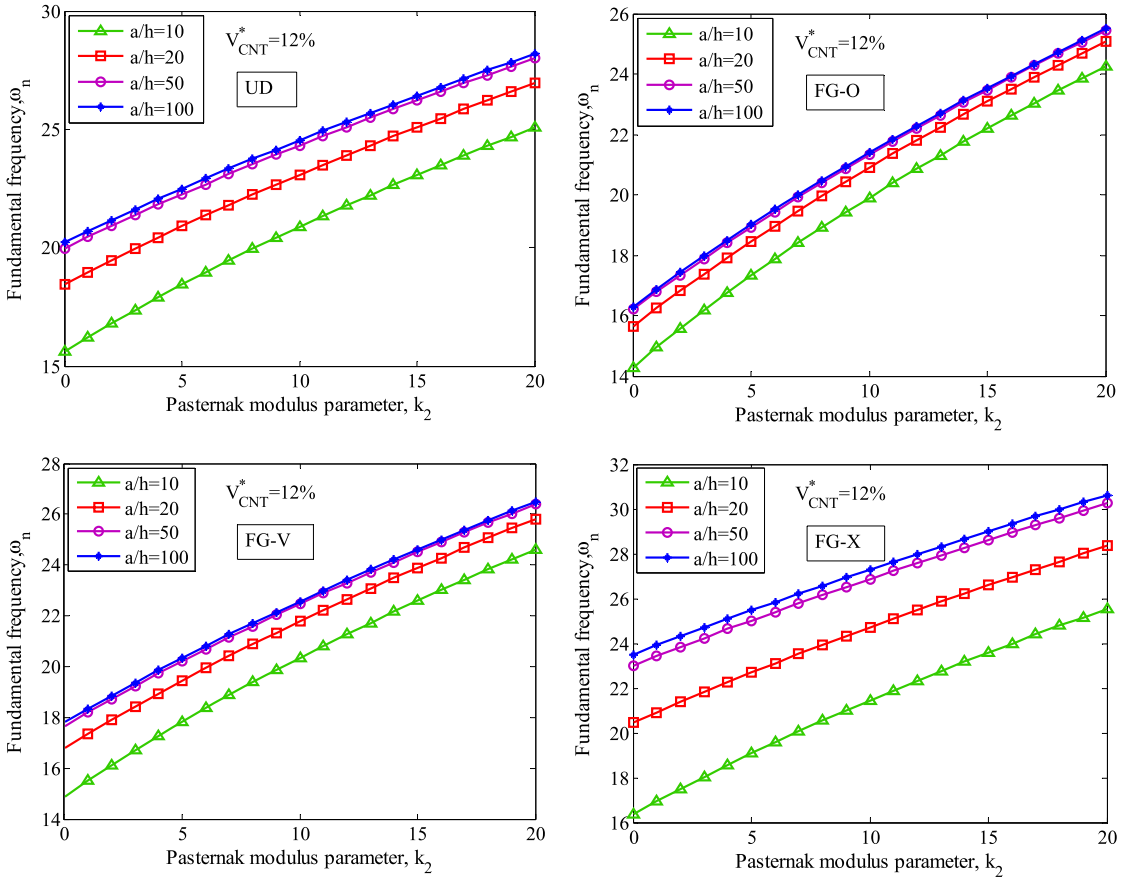

Fig. 10. Effect of the Pasternak modulus parameter, k_2 on the fundamental frequency parameter of the CNTRC plates for various values of a/h ratio ($a/b = 1$, $V^*_{CNT} = 12\%$).

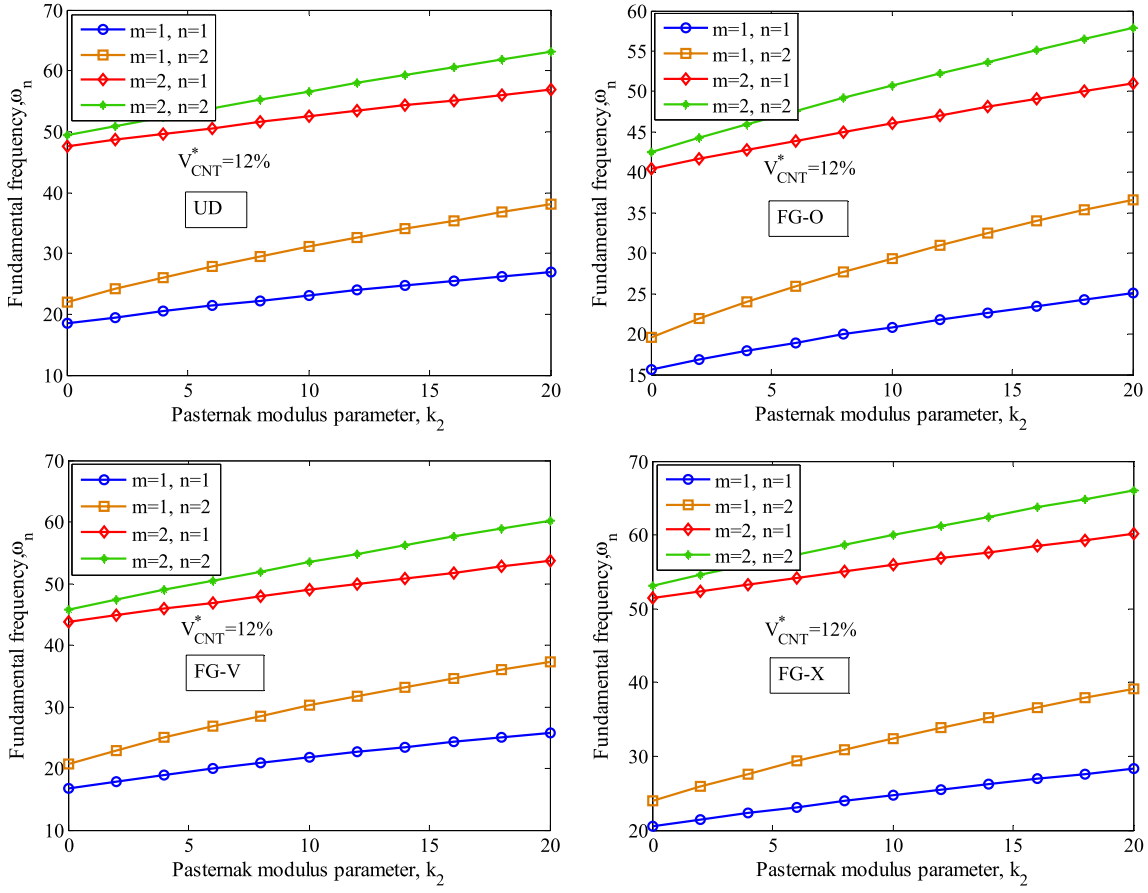

Fig. 11. Effect of the mode (m, n) on the fundamental frequency parameter of the CNTRC plates ($a/b = 1$, $b/h = 20$, $V^*_{CNT} = 12\%$).

the frequency parameters is almost the same for all types of CNTs distributions.

The influence of the Pasternak modulus parameter, k_2 on the first fundamental frequency parameter $\omega_n = \omega^2\sqrt{\rho_m/E_m}/h$ of FG-CNTRC plates for various values of length-to-thickness ratio (a/h), as one of the important geometrical parameters of the plate are indicated in Fig. 10. Finally, Fig. 11 demonstrates the effect of mode number on the variation of the non-dimensional frequency parameter of simply supported FG-CNTRC various values of Pasternak modulus parameter k_2. As depicted, the non-dimensional frequency parameters of the FG-CNTRC plate are strongly affected by the mode number.

6. Concluding remark

In this paper, the authors develop an analytical solution to investigate the static response and free vibration of the simply supported FG-CNTRC rectangular plates resting on Winkler–Pasternak foundation based on the first-order shear deformation plate theory. Some examples are verified to have higher accuracy than those from the previous approach in the literature. From the study, some general observations are summarized as follows:

- Increasing the CNT volume fraction causes to decrease the non-dimensional center deflection.
- Central deflection of FG-X plate has lowest, while the FG-O plate has higher deflection and the UD plate lies between FG-X and FG-O.
- For the vibration problem, fundamental frequency parameter $\omega_n = \omega^2\sqrt{\rho_m/E_m}/h$ in FG-X case are smaller than that other for the other cases of CNT distribution.
- For all type of CNTs distributions, the non-dimensional frequency parameters of the FG-CNTRC plate are strongly affected by the mode number and geometrical parameters.

In addition, the presented results can be used as benchmark solution for future research work.

Conflict of interest statement

The authors declare no conflict of interest.

Acknowledgements

This research was supported by a Grant (NRF-2015R1A2A1A-01007535) from NRF (National Research Foundation of Korea) funded by MEST (Ministry of Education and Science Technology) of Korean government. The support is gratefully acknowledged.

References

[1] S. Iijima, Helical microtubules of graphitic carbon, Nature 354 (1991) 56–58.
[2] M.-F. Yu, B.S. Files, S. Arepalli, R.S. Ruoff, Tensile loading of ropes of single wall carbon nanotubes and their mechanical properties, Phys. Rev. Lett. 84 (2000) 5552–5555.
[3] J.-P. Salvetat, G.A.D. Briggs, J.-M. Bonard, R.R. Bacsa, A.J. Kulik, T. Stöckli, et al., Elastic and shear moduli of single-walled carbon nanotube ropes, Phys. Rev. Lett. 82 (1999) 944–947.
[4] E. Hernández, C. Goze, P. Bernier, A. Rubio, Elastic properties of C and $B_xC_yN_z$ composite nanotubes, Phys. Rev. Lett. 80 (1998) 4502–4505.
[5] C.F. Cornwell, L.T. Wille, Elastic properties of single-walled carbon nanotubes in compression, Solid State Commun. 101 (1997) 555–558.
[6] J.W.G. Wilder, L.C. Venema, A.G. Rinzler, R.E. Smalley, C. Dekker, Electronic structure of atomically resolved carbon nanotubes, Nature 391 (1998) 59–62.

[7] M.-F. Yu, O. Lourie, M.J. Dyer, K. Moloni, T.F. Kelly, R.S. Ruoff, Strength and breaking mechanism of multiwalled carbon nanotubes under tensile load, Science 287 (2000) 637–640.
[8] A. Krishnan, E. Dujardin, T.W. Ebbesen, P.N. Yianilos, M.M.J. Treacy, Young's modulus of single-walled nanotubes, Phys. Rev. B 58 (1998) 14013–14019.
[9] J. Hone, M. Whitney, A. Zettl, Thermal conductivity of single-walled carbon nanotubes, Synth. Met. 103 (1999) 2498–2499.
[10] M.M.J. Treacy, T.W. Ebbesen, J.M. Gibson, Exceptionally high Young's modulus observed for individual carbon nanotubes, Nature 381 (1996) 678–680.
[11] B.Q. Wei, R. Vajtai, P.M. Ajayan, Reliability and current carrying capacity of carbon nanotubes, Appl. Phys. Lett. 79 (2001) 1172–1174.
[12] J. Gou, B. Minaie, B. Wang, Z. Liang, C. Zhang, Computational and experimental study of interfacial bonding of single-walled nanotube reinforced composites, Comput. Mater. Sci. 31 (2004) 225–236.
[13] J.D. Fidelus, E. Wiesel, F.H. Gojny, K. Schulte, H.D. Wagner, Thermo-mechanical properties of randomly oriented carbon/epoxy nanocomposites, Composites, Part A, Appl. Sci. Manuf. 36 (2005) 1555–1561.
[14] G.M. Odegard, T.S. Gates, K.E. Wise, C. Park, E.J. Siochi, Constitutive modeling of nanotube-reinforced polymer composites, Compos. Sci. Technol. 63 (2003) 1671–1687.
[15] A.M.K. Esawi, M.M. Farag, Carbon nanotube reinforced composites: potential and current challenges, Mater. Des. 28 (2007) 2394–2401.
[16] G.D. Seidel, D.C. Lagoudas, Micromechanical analysis of the effective elastic properties of carbon nanotube reinforced composites, Mech. Mater. 38 (2006) 884–907.
[17] Y. Han, J. Elliott, Molecular dynamics simulations of the elastic properties of polymer/carbon nanotube composites, Comput. Mater. Sci. 39 (2007) 315–323.
[18] G. Formica, W. Lacarbonara, R. Alessi, Vibrations of carbon nanotube-reinforced composites, J. Sound Vib. 329 (2010) 1875–1889.
[19] J. Wuite, S. Adali, Deflection and stress behaviour of nanocomposite reinforced beams using a multiscale analysis, Compos. Struct. 71 (2005) 388–396.
[20] N. Hu, H. Fukunaga, C. Lu, M. Kameyama, B. Yan, Prediction of elastic properties of carbon nanotube reinforced composites, Proc. R. Soc. A, Math. Phys. Eng. Sci. 461 (2005) 1685, LP-1710.
[21] P. Bonnet, D. Sireude, B. Garnier, O. Chauvet, Thermal properties and percolation in carbon nanotube-polymer composites, Appl. Phys. Lett. 91 (2007) 201910.
[22] M. Koizumi, Functionally gradient materials the concept of FGM, Ceram. Trans. 34 (1993) 3–10.
[23] Y. Obata, N. Noda, Transient thermal stresses in a plate of functionally gradient material, Ceram. Trans. Funct. Graded Mater. 34 (1993) 403–410.
[24] H.-S. Shen, Nonlinear bending of functionally graded carbon nanotube-reinforced composite plates in thermal environments, Compos. Struct. 91 (2009) 9–19.
[25] Z.X. Lei, L.W. Zhang, K.M. Liew, Buckling of FG-CNT reinforced composite thick skew plates resting on Pasternak foundations based on an element-free approach, Appl. Math. Comput. 266 (2015) 773–791.
[26] L.W. Zhang, Z.G. Song, K.M. Liew, Nonlinear bending analysis of FG-CNT reinforced composite thick plates resting on Pasternak foundations using the element-free IMLS-Ritz method, Compos. Struct. 128 (2015) 165–175.
[27] L.W. Zhang, K.M. Liew, J.N. Reddy, Postbuckling of carbon nanotube reinforced functionally graded plates with edges elastically restrained against translation and rotation under axial compression, Comput. Methods Appl. Mech. Eng. 298 (2016) 1–28.
[28] Z.X. Lei, K.M. Liew, J.L. Yu, Free vibration analysis of functionally graded carbon nanotube-reinforced composite plates using the element-free *kp*-Ritz method in thermal environment, Compos. Struct. 106 (2013) 128–138.
[29] L.W. Zhang, W.C. Cui, K.M. Liew, Vibration analysis of functionally graded carbon nanotube reinforced composite thick plates with elastically restrained edges, Int. J. Mech. Sci. 103 (2015) 9–21.
[30] L.W. Zhang, Z.X. Lei, K.M. Liew, Free vibration analysis of functionally graded carbon nanotube-reinforced composite triangular plates using the FSDT and element-free IMLS-Ritz method, Compos. Struct. 120 (2015) 189–199.
[31] L.W. Zhang, Z.X. Lei, K.M. Liew, Vibration characteristic of moderately thick functionally graded carbon nanotube reinforced composite skew plates, Compos. Struct. 122 (2015) 172–183.
[32] Z.G. Song, L.W. Zhang, K.M. Liew, Vibration analysis of CNT-reinforced functionally graded composite cylindrical shells in thermal environments, Int. J. Mech. Sci. 115 (2016) 339–347.
[33] P. Phung-Van, M. Abdel-Wahab, K.M. Liew, S.P.A. Bordas, H. Nguyen-Xuan, Isogeometric analysis of functionally graded carbon nanotube-reinforced composite plates using higher-order shear deformation theory, Compos. Struct. 123 (2015) 137–149.
[34] P.T. Thang, T.-T. Nguyen, J. Lee, A new approach for nonlinear buckling analysis of imperfect functionally graded carbon nanotube-reinforced composite plates, Composites, Part B, Eng. (2016).
[35] N.D. Duc, P.H. Cong, N.D. Tuan, P. Tran, N. Van Thanh, Thermal and mechanical stability of functionally graded carbon nanotubes (FG CNT)-reinforced composite truncated conical shells surrounded by the elastic foundations, Thin-Walled Struct. 115 (2017) 300–310.
[36] H.-S. Shen, Postbuckling of nanotube-reinforced composite cylindrical shells in thermal environments, Part I: axially-loaded shells, Compos. Struct. 93 (2011) 2096–2108.
[37] H.-S. Shen, Postbuckling of nanotube-reinforced composite cylindrical shells in thermal environments, Part II: pressure-loaded shells, Compos. Struct. 93 (2011) 2496–2503.
[38] H.-S. Shen, Torsional postbuckling of nanotube-reinforced composite cylindrical shells in thermal environments, Compos. Struct. 116 (2014) 477–488.
[39] H.-S. Shen, Y. Xiang, Postbuckling of nanotube-reinforced composite cylindrical shells under combined axial and radial mechanical loads in thermal environment, Composites, Part B, Eng. 52 (2013) 311–322.
[40] L.-L. Ke, J. Yang, S. Kitipornchai, Nonlinear free vibration of functionally graded carbon nanotube-reinforced composite beams, Compos. Struct. 92 (2010) 676–683.
[41] A. Alibeigloo, Static analysis of functionally graded carbon nanotube-reinforced composite plate embedded in piezoelectric layers by using theory of elasticity, Compos. Struct. 95 (2013) 612–622.
[42] A. Alibeigloo, Three-dimensional thermoelasticity solution of functionally graded carbon nanotube reinforced composite plate embedded in piezoelectric sensor and actuator layers, Compos. Struct. 118 (2014) 482–495.
[43] C.-P. Wu, S.-K. Chang, Stability of carbon nanotube-reinforced composite plates with surface-bonded piezoelectric layers and under bi-axial compression, Compos. Struct. 111 (2014) 587–601.
[44] R. Ansari, E. Hasrati, M. Faghih Shojaei, R. Gholami, A. Shahabodini, Forced vibration analysis of functionally graded carbon nanotube-reinforced composite plates using a numerical strategy, Physica E, Low-Dimens. Syst. Nanostruct. 69 (2015) 294–305.
[45] S.K. Jalali, M. Heshmati, Buckling analysis of circular sandwich plates with tapered cores and functionally graded carbon nanotubes-reinforced composite face sheets, Thin-Walled Struct. 100 (2016) 14–24.
[46] Y. Kiani, Free vibration of FG-CNT reinforced composite skew plates, Aerosp. Sci. Technol. 58 (2016) 178–188.
[47] Y. Kiani, Shear buckling of FG-CNT reinforced composite plates using Chebyshev–Ritz method, Composites, Part B, Eng. 105 (2016) 176–187, http://dx.doi.org/10.1016/j.compositesb.2016.09.001.
[48] R. Ansari, J. Torabi, A. Hosein Shakouri, Vibration analysis of functionally graded carbon nanotube-reinforced composite elliptical plates using a numerical strategy, Aerosp. Sci. Technol. 60 (2017) 152–161.
[49] J.N. Reddy, Mechanics of Laminated Composite Plates and Shells: Theory and Analysis, CRC Press, 2004.
[50] P. Zhu, Z.X. Lei, K.M. Liew, Static and free vibration analyses of carbon nanotube-reinforced composite plates using finite element method with first order shear deformation plate theory, Compos. Struct. 94 (2012) 1450–1460.
[51] L.W. Zhang, Z.X. Lei, K.M. Liew, Computation of vibration solution for functionally graded carbon nanotube-reinforced composite thick plates resting on elastic foundations using the element-free IMLS-Ritz method, Appl. Math. Comput. 256 (2015) 488–504.